



Published in final edited form as:

*Magn Reson Med.* 2023 October ; 90(4): 1363–1379. doi:10.1002/mrm.29713.

## Robust cardiac $T_{1\rho}$ mapping at 3T using adiabatic spin-lock preparations

Chiara Coletti<sup>1</sup>, Anastasia Fotaki<sup>2</sup>, Joao Tourais<sup>1</sup>, Yidong Zhao<sup>1</sup>, Christal van de Steeg-Henzen<sup>3</sup>, Mehmet Akçakaya<sup>4</sup>, Qian Tao<sup>1</sup>, Claudia Prieto<sup>2,5,6</sup>, Sebastian Weingärtner<sup>1</sup>

<sup>1</sup>Department of Imaging Physics, Delft University of Technology, Delft, The Netherlands

<sup>2</sup>Department of Biomedical Engineering, King's College London, London, United Kingdom

<sup>3</sup>HollandPTC, Delft, The Netherlands

<sup>4</sup>Department of Electrical and Computer Engineering and Center for Magnetic Resonance Research, University of Minnesota, Minnesota, USA

<sup>5</sup>School of Engineering, Pontificia Universidad Católica de Chile, Santiago, Chile

<sup>6</sup>Millenium Institute for Intelligent Healthcare Engineering, Santiago, Chile

### Abstract

**Purpose:** To develop and optimize an adiabatic  $T_{1\rho}(T_{1\rho, \text{adiab}})$  mapping method for robust quantification of spin-lock (SL) relaxation in the myocardium at 3T.

**Methods:** Adiabatic SL (aSL) preparations were optimized for resilience against  $B_0$  and  $B_1^+$  inhomogeneities using Bloch simulations. Optimized  $B_0$ -aSL, Bal-aSL and  $B_1$ -aSL modules, each compensating for different inhomogeneities, were first validated in phantom and human calf. Myocardial  $T_{1\rho}$  mapping was performed using a single breath-hold cardiac-triggered bSSFP-based sequence. Then, optimized  $T_{1\rho, \text{adiab}}$  preparations were compared to each other and to conventional SL-prepared  $T_{1\rho}$  maps (RefSL) in phantoms to assess repeatability and in thirteen healthy subjects to investigate image quality, precision, reproducibility and inter-subject variability. Finally, aSL and RefSL sequences were tested on six patients with known or suspected cardiovascular disease and compared with LGE,  $T_1$  and  $T_2$  mapping.

**Results:** The highest  $T_{1\rho, \text{adiab}}$  preparation efficiency was obtained in simulations for modules comprising 2 HS pulses of 30ms each. In vivo  $T_{1\rho, \text{adiab}}$  maps yielded significantly higher quality than RefSL maps. Average myocardial  $T_{1\rho, \text{adiab}}$  values were  $183.28 \pm 25.53$ ms, compared with  $38.21 \pm 14.37$ ms RefSL-prepared  $T_{1\rho}$ .  $T_{1\rho, \text{adiab}}$  maps showed a significant improvement in precision (avg.  $14.47 \pm 3.71\%$  aSL,  $37.61 \pm 19.42\%$  RefSL,  $p < 0.01$ ) and reproducibility (avg.  $4.64 \pm 2.18\%$  aSL,  $47.39 \pm 12.06\%$  RefSL,  $p < 0.0001$ ), with decreased inter-subject variability (avg.  $8.76 \pm 3.65\%$  aSL,  $51.90 \pm 15.27\%$  RefSL,  $p < 0.0001$ ). Among aSL preparations,  $B_0$ -aSL achieved the highest inter-subject variability. In patients,  $B_1$ -aSL preparations showed the best artifact resilience

**Correspondence:** Sebastian Weingärtner, Lorentzweg 1, 2628, CJ, Delft, The Netherlands. s.weingartner@tudelft.nl.

SUPPORTING INFORMATION

The following supporting information is available as part of the online article:

among the adiabatic preparations.  $T_{1\rho, \text{adiab}}$  times show focal alteration colocalized with areas of hyperenhancement in the LGE images.

**Conclusion:** Adiabatic preparations enable robust in vivo quantification of myocardial SL relaxation times at 3T.

### Keywords

$T_{1\rho}$  mapping; spin-lock relaxation; adiabatic RF;  $B_0/B_1^+$  inhomogeneities; myocardium

## 1 | INTRODUCTION

Cardiac MRI is the clinical gold standard for the assessment of scar and fibrosis in ischemic and non-ischemic heart diseases<sup>1,2,3,4</sup>. Late gadolinium enhancement (LGE) imaging can be used to differentiate between scar and healthy myocardium based on retention of gadolinium-based contrast agents (GBCA)<sup>5</sup>. However, GBCAs injection is contraindicated in patients with severe renal impairment due to the risk of necrotic systemic fibrosis<sup>6</sup>. In addition, gadolinium retention in the brain after injection of GBCAs has been reported<sup>7</sup>. Thus, contrast-free alternatives are highly desired.

Quantitative myocardial tissue characterization has emerged with a wide spectrum of applications in various cardiomyopathies<sup>8</sup>. Native  $T_1$  mapping has been explored for the assessment of myocardial infarction (MI) without the need for contrast agents<sup>9,10,11</sup>. However, mixed results have been reported on its sensitivity to focal scar and the approach remains the subject of ongoing research<sup>12,13,14</sup>.

$T_{1\rho}$  mapping has been proposed as a promising non-contrast alternative for scar assessment, due to its increased sensitivity to slow molecular motion in the kilohertz range<sup>15,16</sup>. First, Muthupillai et al. reported stronger post-contrast enhancement in acute MI cases for  $T_{1\rho}$ -weighted imaging compared with conventional  $T_1$ -weighted LGE imaging<sup>17,18</sup>. More recently, quantitative  $T_{1\rho}$  maps have demonstrated improved differentiation between infarcted and remote myocardium in swine models, compared with native  $T_1$  and  $T_2$  maps, yielding comparable contrast-to-noise ratio (CNR) to LGE images<sup>19,20,13</sup>. Similar results have been reported in mice<sup>21,22,23</sup> and monkeys<sup>24</sup>. In vivo  $T_{1\rho}$  mapping has been successfully applied in patients with ischemic and non-ischemic cardiomyopathies at 1.5T<sup>25,26,27,28,29,30</sup>. Implementing  $T_{1\rho}$  mapping at 3T could further improve the diagnostic value of this approach, due to an increase in signal-to-noise ratio (SNR) and CNR, and the applicability in a growing number of 3T cardiac examinations. However, at 3T, only a few studies have been reported<sup>31,32,33</sup>, highlighting limitations related to system imperfections and the specific absorption rate (SAR) at high field strengths.

Conventional  $T_{1\rho}$  maps are obtained using spin-lock (SL) preparation pulses with various durations, which are most commonly based on continuous-wave RF irradiation. These preparations are inherently susceptible to  $B_0$  and  $B_1^+$  field inhomogeneities<sup>34,35</sup>. To compensate for these inhomogeneities, continuous-wave SL pulses, in combination with refocusing pulses and phase cycling of SL modules, have been proposed<sup>36,34,37</sup>.

An alternative strategy to achieve resilience against system imperfections is the use of adiabatic pulses<sup>38</sup>. The robustness of adiabatic pulses against field inhomogeneities has been studied in other 3T cardiac MRI methods, such as inversion-recovery  $T_1$  mapping<sup>39</sup> or refocusing in  $T_2$  preparations<sup>40</sup>. Recently, similar adiabatic pulses have also been employed for refocusing in conventional SL preparations for cardiac  $T_{1\rho}$  mapping<sup>29</sup> at 1.5T. Alternatively, SL preparations consisting of trains of adiabatic full passage (AFP) pulses have been proposed to generate  $T_{1\rho}$  contrast in other anatomies<sup>41,42</sup>. During the AFP frequency sweep, the magnetization is locked along the effective field. This induces  $T_{1\rho, \text{adiab}}$  as the dominant relaxation mechanism during the pulse application<sup>43,44</sup>.  $T_{1\rho, \text{adiab}}$  will be used throughout the manuscript to indicate the rotating frame of reference relaxation constant measured by adiabatic preparations.

In this work, we sought to investigate the use of fully adiabatic SL (aSL) preparations for  $T_{1\rho, \text{adiab}}$  mapping of the myocardium at 3T. Bloch simulations were performed to optimize aSL pulse shapes for resilience against system imperfections. Phantom and in vivo imaging of the calf muscle were then carried out to compare aSL preparations against fully compensated conventional SL preparations. In vivo performance was shown with cardiac mapping in healthy subjects. Finally, clinical feasibility was evaluated in a small proof-of-principle cohort of patients.

## 2 | METHODS

### 2.1 | Adiabatic spin-lock preparation design

In this work, adiabatic SL (aSL) preparations were based on a train of AFP pulses with an identical duration (Fig. 1 B). An even number of pulses was used to ensure that, at the end of the preparation ( $t = \tau_{\text{sl}}$ ), the magnetization  $M(\tau_{\text{sl}})$  was stored along the  $+z$  direction. Hyperbolic secant (HS) pulse shapes were employed, as commonly used in other imaging applications<sup>40,39,41,45,46</sup>. These are characterized by the following amplitude and frequency modulation functions:

$$B_1(t) = B_1^{\text{max}} \cdot \text{sech}\left(\beta\left(\frac{2t}{\tau_{\text{HS}}} - 1\right)\right), \quad (1)$$

$$\Delta\omega_1(t) = \omega_1(t) - \omega_0 = 2f_{\text{max}} \cdot \tanh\left(\beta\left(\frac{2t}{\tau_{\text{HS}}} - 1\right)\right). \quad (2)$$

Here  $B_1(t)$  represents the pulse amplitude,  $B_1^{\text{max}}$  the peak amplitude, and  $\beta$  a constant that characterizes the width of the pulse bell. The single HS pulse duration is indicated by  $\tau_{\text{HS}}$ .  $\Delta\omega_1(t)$  is the frequency modulation with respect to the Larmor frequency  $\omega_0$ ,  $2f_{\text{max}}$  is the amplitude of the frequency sweep, and  $\Delta\omega_1(t) = d\Phi_1(t)/dt$ , where  $\Phi_1(t)$  represents the pulse phase as a function of time. The polarity of the frequency sweep was alternated between consecutive HS pulses to compensate for residual pulse imperfections.

Preparations with variable SL durations were achieved by concatenating identical pulse modules multiple times. The total duration of a single aSL module ( $\tau_{SL}$ ) was fixed to 60 ms. This value was chosen as a trade-off between adequate sampling of the expected range of in vivo  $T_{1\rho, \text{adiab}}$  times and restrictions imposed by the SAR limits (whole-body SAR < 2.0 W/kg) and the RF amplifier chain. To obtain constant preparation times, when changing the pulse duration ( $\tau_{HS}$ ), modules containing 2, 4 or 8 HS pulses (2HS-aSL, 4HS-aSL, 8HS-aSL) with relative pulse duration  $\tau_{SL}$ ,  $\tau_{SL}/2$ , and  $\tau_{SL}/4$ , were implemented. For SL modules with 4 and 8 HS pulses, phase cycling was adopted between pairs of HS pulses to achieve a full Malcolm-Levitt (MLEV) scheme compensation<sup>47</sup>.

**2.1.1 | Bloch simulations**—Bloch simulations were used to optimize  $\beta$ ,  $f_{\max}$  and  $\tau_{HS}$  in the aSL preparations. All simulations were performed in MATLAB (MathWorks, Natick, USA).

The preparation efficiency was determined as  $M_z(\tau_{SL})/M(0)$  and used as a metric to optimize the design of the aSL module. The aSL preparation modules were simulated using the maximum RF pulse power, within the limits imposed by the peak  $B_1^+$  ( $B_1^{\max} = 13.5\mu\text{T}$ ) and SAR (whole-body SAR < 2.0 W/kg). The preparation efficiency was averaged over a design window covering the expected range of in vivo off-resonances ( $\Delta\omega_1^{\text{off}} \in \{-150, -149, \dots, +150\}\text{Hz}$ ) and  $B_1^+$  inhomogeneities ( $\zeta_1 \in \{0.50, 0.49, \dots, 1.00\}$ )<sup>48,63,62?</sup> where  $\zeta_1$  indicates the ratio between the effective and nominal  $B_1^+$  power.

Two sets of optimizations were performed to identify the optimal pulse duration and amplitude/frequency modulation functions, respectively. First, the 2HS-aSL, 4HS-aSL, and 8HS-aSL modules were compared in terms of preparation efficiency. Then, the module that produced the highest preparation efficiency was selected to derive the optimal values of  $\beta$  and  $f_{\max}$ . Bloch simulations covering the range of expected in vivo variability of  $B_0$  and  $B_1^+$  were performed to obtain optimized pulses for three design regions: 1) original balanced design region (Bal-aSL) ( $\Delta\omega_1^{\text{off}} \in \{-150, -149, \dots, +150\}\text{Hz}$ ,  $\zeta_1 \in \{0.50, 0.49, \dots, 1.00\}$ ); 2)  $B_0$ -skewed ( $B_0$ -aSL) ( $\Delta\omega_1^{\text{off}} \in \{-200, -199, \dots, +200\}\text{Hz}$ ,  $\zeta_1 \in \{0.75, 0.76, \dots, 1.00\}$ ); 3)  $B_1^+$ -skewed design regions ( $B_1^+$ -aSL) ( $\Delta\omega_1^{\text{off}} \in \{-100, -99, \dots, +100\}\text{Hz}$ ,  $\zeta_1 \in \{0.25, 0.26, \dots, 1.00\}$ ).

**2.1.2 | Pulse design validation**—Phantom data were acquired to validate the simulation results. The preparation efficiency of three optimized SL modules  $B_0$ -aSL, Bal-aSL, and  $B_1^+$ -aSL was tested on the phantom by modifying the center frequency  $\Delta\omega_1^{\text{off}} \in \{-200, -180, \dots, +200\}\text{Hz}$  and scaling the pulse power by  $\zeta_1 \in \{0.1, 0.2, \dots, 1.0\}$ . A single bottle phantom (Spectrasyn 4 polyalphaolefin, ExxonMobil Chemical) was used for the experiments.

The same experiments were performed in vivo in the calf muscle of a healthy subject (21 y.o.) to validate simulations and phantom experiments for the three aSL preparations. Here,  $B_0$  and  $B_1^+$  inhomogeneities were varied in fewer steps ( $\Delta\omega_1^{\text{off}} \in \{-200, -150, \dots, +200\}\text{Hz}$ ,  $\zeta_1 \in \{0.2, 0.4, \dots, 1.0\}$ ).

For each SL module,  $\Delta\omega_1^{\text{off}}$  and  $\zeta_1$ , two snap-shot balanced steady-state free-precession (bSSFP) images were acquired: one preceded by the aSL preparation ( $\tau_{\text{SL}} = 60$  ms) and one with no preparation. The two scans were interleaved by a 5s pause to allow longitudinal magnetization recovery. Low imaging resolution was used ( $10 \times 10 \times 10$  mm<sup>3</sup>), with  $T = 1.9$ ms,  $TE = 0.72$ ms R, flip angle =  $90^\circ$  and a SENSE factor of 2. The preparation efficiency  $M_z(\tau_{\text{SL}})/M(0)$  was then calculated as the ratio of the two magnitude images. Signal polarity was restored using the corresponding phase images prior to further processing. In phantoms, the entire phantom area was evaluated for each vial, while in the calf, manually drawn circular regions-of-interest (ROIs) were used.

## 2.2 | $T_{1\rho}$ mapping

The proposed  $T_{1\rho, \text{adiab}}$  mapping approaches were compared to each other and to a conventional, continuous-wave  $T_{1\rho}$  mapping implementation in phantom and through in vivo experiments in the calf muscle and the myocardium in healthy subjects and patients. Phantoms and healthy subjects were scanned on a 3T Ingenia system (Philips, Best, The Netherlands). Patient data was acquired on a 3T Achieva system (Philips, Best, The Netherlands). In vivo imaging was ethically approved by the competent review authorities (METC NL73381.078.20, UK National Research Ethics Service 15/NS/0030). Written informed consent has been obtained prior to all imaging sessions according to institutional guidelines.

The aSL preparations were compared to a fully balanced non-adiabatic SL pulse<sup>37</sup> (RefSL in Fig. 1 A). Three phasecycled SL blocks with equal amplitude and durations of  $\tau_{\text{SL}}/4$ ,  $\tau_{\text{SL}}/2$ , and  $\tau_{\text{SL}}/4$ , respectively, were played. The SL amplitude was chosen based on the RF amplifier constraints as  $B_1^+/\gamma = 300$  Hz.

$T_{1\rho}$  and  $T_{1\rho, \text{adiab}}$  mapping was performed using a cardiac triggered breath-hold sequence (Fig. 2). Five baseline single-shot bSSFP images were acquired: the first with no SL preparation, then three with increasing SL durations, and finally a saturation-prepared image used to approximate infinite SL length<sup>49</sup>. A composite “Water suppression Enhanced through T1-effects” (WET) pulse was used to achieve robust saturation in the presence of field inhomogeneities<sup>61</sup>. Total preparation durations were  $\tau_{\text{SL}} = 0, 60, 120, 180$  ms for aSL modules. Shorter preparations were employed for RefSL ( $\tau_{\text{SL}} = 0, 12, 24, 36$  ms) to account for higher SAR levels, heavier RF amplifier load, and significantly shorter non-adiabatic  $T_{1\rho}$  times. Scans were acquired in the end-diastolic phase. All images, except the saturation-prepared image, were preceded by a pause to allow for longitudinal magnetization recovery. Other imaging parameters were: in-plane resolution =  $2 \times 2$ mm<sup>2</sup>, FOV =  $220 \times 220$ mm<sup>2</sup>, slice thickness = 8mm, TE/TR = 1.2/2.4ms, flip angle =  $70^\circ$ , SENSE = 2.

$T_{1\rho}$  and  $T_{1\rho, \text{adiab}}$  maps were reconstructed in MATLAB using the following three-parameter model<sup>49</sup>, to account for the effect of the imaging pulses:

$$S(t) = A \cdot e^{-\frac{t}{T_{1\rho, \text{adiab}}}} + B.$$

(3)

**2.2.1 | Phantom and in-vivo calf experiments**—The TIMES phantom was used for phantom experiments to mimic blood and myocardium relaxation times at  $3T^{60}$ . Approximate  $T_1$  and  $T_2$  times of the phantom vials were estimated, using a MOLLI sequence for  $T_1$  and a Gradient Spin Echo (GraSE) sequence for  $T_2$ . To study repeatability, ten repetitions of  $T_{1\rho}$  and  $T_{1\rho, \text{adiab}}$  mapping scans were acquired for each preparation ( $B_0$ -aSL, Bal-aSL,  $B_1$ -aSL and RefSL). Manually drawn circular ROIs were used to extract  $T_{1\rho}$  and  $T_{1\rho, \text{adiab}}$  values for further processing. Repeatability was assessed using the coefficient of variability ( $\bar{C}V$ ):

$$\bar{C}V = \sum_{i=1}^{N_v} \frac{w\bar{C}V_i}{N_v} \quad (4)$$

where  $N_v$  is the number of samples, corresponding to the number of vials in this case, and  $w\bar{C}V_i$  is the coefficient of variability within the sample computed for every vial as:

$$w\bar{C}V_i = \frac{1}{R} \sum_{r=1}^R \frac{\sqrt{(\mu_{i,r} - \bar{\mu}_i)^2}}{\bar{\mu}_i}. \quad (5)$$

Here,  $R = 10$  represents the number of repetitions,  $\mu_{i,r}$  is the average  $T_{1\rho}$  or  $T_{1\rho, \text{adiab}}$  value for each vial  $i$  and repetition  $r$  and  $\bar{\mu}_i$  is the average  $T_{1\rho}$  or  $T_{1\rho, \text{adiab}}$  value for each vial across all repetitions.

In a second experiment,  $T_{1\rho, \text{adiab}}$  time was assessed as a function of the HS shape parameter  $\beta$  by acquiring phantom and calf  $T_{1\rho, \text{adiab}}$  maps for  $\beta \in 1, 2, \dots, 10$ . For each  $\beta$ , a constant sweep amplitude  $f_{\text{max}}$  value was acquired. The dependence between the parameter  $\beta$  and the measured  $T_{1\rho, \text{adiab}}$  values was tested using linear regression.  $R^2$  coefficient, slope and intercept values were reported for a single exemplary vial and a manually drawn circular calf ROI.

**2.2.2 | Healthy subjects experiments**—The proposed aSL preparations were tested in 6 healthy subjects (4 males, 2 females,  $21.5 \pm 1.9$  y.o.). For each subject,  $B_0$ -aSL, Bal-aSL, and  $B_1$ -aSL  $T_{1\rho, \text{adiab}}$  maps were acquired in three short-axis (SAX) slices (basal, mid, and apical) and a four-chamber (4ch) view. To assess reproducibility, the twelve maps were re-acquired following the repositioning of the subject<sup>51</sup>. In this cohort of healthy subjects, the magnetization recovery pause was 2.5s to limit the total scan time to 13s.

In a second cohort of 7 healthy subjects (5 males, 2 females,  $24.7 \pm 2.5$  y.o.), the best-performing aSL preparation was compared to RefSL. Similarly to the first cohort, three SAX slices and a 4ch view were acquired for each subject and preparation. Here, a magnetization recovery pause of 3.5s was employed to avoid relaxation time over-estimation

(see Supporting Information Fig. S1). To assess robustness to  $B_0$  and  $B_1^+$  inhomogeneities, a second repetition of each map was acquired by moving the shimming volume only on the right ventricle, while keeping the position of the patient fixed.

The myocardium was automatically segmented using the nnU-Net framework<sup>52</sup> with uncertainty estimation<sup>53</sup>. Segmentation maps with predictive confidence below 75% were discarded and the segmentation was performed manually. The average values of  $T_{1\rho}$  or  $T_{1\rho, \text{adiab}}$  and their corresponding standard deviation values (std) in the segmented myocardium were extracted according to the AHA 16 segment model. A group-wise ANOVA test followed by paired t-tests were used to assess statistical differences between the  $T_{1\rho}$  and  $T_{1\rho, \text{adiab}}$  times with different preparations.

$T_{1\rho}$  and  $T_{1\rho, \text{adiab}}$  quantification precision was assessed for each myocardial segment and SL module through the within-subject coefficient of variability ( $wCV$ ):

$$wCV_{r,i} = \frac{\sqrt{\sigma_{r,i}^2}}{\mu_{r,i}} \quad (6)$$

computed for every repetition  $r$  and subject  $i$ , where  $\mu$  and  $\sigma$  are the  $T_{1\rho}$  or  $T_{1\rho, \text{adiab}}$  mean and std, respectively. Then, the mean and std of  $T_{1\rho}$  or  $T_{1\rho, \text{adiab}}$  values across repetitions were computed as:

$$\bar{\mu}_i = \sum_{r=1}^R \frac{\mu_{r,i}}{R}, \quad \bar{\sigma}_i = \frac{1}{R} \sqrt{\sum_{r=1}^R (\mu_{r,i} - \bar{\mu}_i)^2} \quad (7)$$

and, therefore, the reproducibility as:

$$w\bar{C}V_i = \bar{\sigma}_i / \bar{\mu}_i, \quad (8)$$

where  $R=2$  indicates the number of repetitions. Finally, the inter-subject variability was computed as a summary of the deviation of each subject's average  $T_{1\rho}$  or  $T_{1\rho, \text{adiab}}$  value from the overall mean:

$$\bar{C}V = \bar{\bar{\sigma}} / \bar{\bar{\mu}}, \quad (9)$$

where

$$\bar{\bar{\mu}} = \sum_{i=1}^N \frac{\bar{\mu}_i}{N_s}, \quad \bar{\bar{\sigma}} = \frac{1}{N_s} \sqrt{\sum_{i=1}^N (\bar{\mu}_i - \bar{\bar{\mu}})^2}$$

(10)

and  $N_s$  indicates the number of subjects. Statistical differences between the different SL preparations in terms of precision and reproducibility were investigated using a group-wise Kruskal-Wallis test and subsequently right-tailed pair-wise Mann-Whitney U-tests.

**2.2.3 | Patients experiments**—Clinical feasibility was tested in a small proof-of-principle cohort of 6 patients (2 males, 4 females,  $50.2 \pm 11.0$  y.o.) referred to clinical CMR. All patients were imaged using standard clinical protocols, including MOLLI-based native  $T_1$  mapping, LGE imaging and CINE scans. LGE imaging was performed 10–15 minutes after injection of 0.15 mmol/kg of Gadobutrol (Gadovist, Bayer Schering, Berlin, Germany). In 4 of the 6 patients, native  $T_2$  maps were also acquired with a Gradient Spin Echo (GraSE) sequence<sup>7</sup>. The proposed  $T_{1\rho, \text{adiab}}$  mapping sequence and conventional  $T_{1\rho}$  mapping of a single mid-ventricular SAX slice were included in the scan protocol prior to contrast administration. Imaging parameters were chosen to closely match those used in the healthy subjects. PCA-based group-wise registration was used to mitigate residual cardiac and respiratory motion for baseline  $T_{1\rho, \text{adiab}}$  and  $T_{1\rho}$  images<sup>59</sup>. Manually drawn ROIs were defined to extract scar and remote  $T_1$ ,  $T_{1\rho, \text{adiab}}$ , and  $T_{1\rho}$  times.

### 3 | RESULTS

#### 3.1 | Bloch simulations results

The simulated preparation efficiency achieved with the 2HS-aSL, 4HS-aSL and 8HS-aSL preparations is shown in Fig. 3 A. For all three modules, the highest preparation efficiency was obtained for low to intermediate frequency sweep amplitudes and showed an inversely proportional relationship with the parameter  $\beta$ . However, very low values of  $\beta$  required a reduction of the pulse peak power to satisfy SAR limitations. In all three cases, the optimal region is well defined and separated from the non-adiabatic region at high sweep velocities (top-right corner). Overall, 2HS-aSL shows higher overall preparation efficiency than 4HS-aSL and 8HS-aSL. The 2HS-aSL module also presents a larger optimal region, indicating higher stability to the choice of parameters. Optimal values of  $\{\beta, f_{\text{max}}\}$  were chosen as  $\{5.5, 350 \text{ Hz}\}$  for 2HS-aSL,  $\{3.7, 300 \text{ Hz}\}$  for 4HS-aSL and  $\{2.1, 550 \text{ Hz}\}$  for 8HS-aSL, resulting in an average efficiency  $M_z/M_0$  of 0.98 and 0.92 and 0.88 respectively. Hence, the 2HS-aSL configuration, consisting of 2 HS pulses of 30ms each, was selected for further investigation.

Simulation results for 2HS-aSL preparation with three different design regions are shown in Fig. 3 B. For  $B_0$ -aSL and  $B_1$ -aSL, similar patterns to the previously analyzed Bal-aSL case (Fig. 3 A) can be observed, with an inversely proportional relationship with the parameter  $\beta$ . The optimal region becomes narrower when using a more  $B_1^+$  compensated preparation, with overall decreasing optimal values  $\beta$  and  $f_{\text{max}}$ . Optimal values of  $\{\beta, f_{\text{max}}\}$  were identified as  $\{6.9, 450 \text{ Hz}\}$  for  $B_0$ -aSL and  $\{4.4, 200 \text{ Hz}\}$  for  $B_1$ -aSL, yielding an average efficiency  $M_z/M_0$  of 0.99 and 0.94 respectively. A summary of the parameters used for the optimized aSL preparations can be found in Table 1.



Fig. 3 C illustrates how the preparation efficiency  $M_z(\tau_{SL})/M(0)$  varies over a range of off-resonant frequencies and  $B_1^+$  inhomogeneities for the optimized  $B_0$ -aSL, Bal-aSL and  $B_1$ -aSL modules according to Bloch simulations. The corresponding design region used for the parameter optimization of each preparation is marked by the dashed rectangle. For all three aSL modules, the regions characterized by low preparation efficiency (in blue) are outside the design region.

### 3.2 | Phantom and in vivo calf experiments

The experimental preparation efficiency measured in the phantom experiments with varying  $\Delta\omega_1^{\text{off}}$  and  $\zeta_1$  conditions is depicted in Fig. 4 A. Good agreement between the simulated and experimental results can be observed. Broad areas of lower preparation efficiency are present for intermediate to low  $\zeta_1$  values with  $B_0$ -aSL, low to very-low  $\zeta_1$  values with Bal-aSL, and very low  $\zeta_1$  as well as high absolute  $\Delta\omega_1^{\text{off}}$  values with  $B_1$ -aSL.

The results of preparation efficiency obtained in vivo in the calf muscle of a healthy subject are shown in Fig. 4 B. These results are in good agreement with both simulations and phantom data. In vivo preparation efficiency is compromised for  $\zeta_1 < 0.6$  with the  $B_0$ -aSL module, while no substantial degradation was observed over the entire off-resonance range studied. On the opposite side,  $B_1$ -aSL yields robust preparation efficiency for  $\zeta_1$  values down to 0.2, but lower efficiency for  $|\Delta\omega_1^{\text{off}}| > 150$  Hz. The overall efficiency score measured in the phantom and calf experiments is lower than in simulations, as no relaxation contributions have been simulated.

Complete  $T_{1\rho}$  and  $T_{1\rho, \text{adiab}}$  mapping results for the TIMES phantom can be found in Supporting Information Fig. S2. Improved repeatability was observed ( $p < 0.05$ ) in  $T_{1\rho, \text{adiab}}$  maps ( $w\bar{C}V_i = 0.29 \pm 0.15$  for  $B_0$ -aSL,  $p < 0.01$ ;  $w\bar{C}V_i = 0.23 \pm 0.13$  for Bal-aSL,  $p < 0.01$ ;  $w\bar{C}V_i = 0.21 \pm 0.11$  for  $B_1$ -aSL,  $p < 0.001$ ) with respect to conventional  $T_{1\rho}$  maps ( $w\bar{C}V_i = 1.30 \pm 1.34$ ) for RefSL).

In Fig. 5, examples of phantom and calf  $T_{1\rho, \text{adiab}}$  maps acquired with different  $\beta$  values are displayed.  $T_{1\rho, \text{adiab}}$  values increase with an approximately linear trend for higher  $\beta$  in both cases ( $R^2 = 0.99$ , slope = 9.56, intercept = 32.15 for phantoms,  $R^2 = 0.91$ , slope = 12.46, intercept = 26.53 for the calf). A higher deviation from linearity was observed in the calf values for  $\beta \in 3, 4, 5$ .

### 3.3 | Healthy subjects experiments

Fig. 6 A shows mid-ventricular SAX and 4ch  $T_{1\rho, \text{adiab}}$  maps for one representative subject, displaying overall strong myocardium-to-blood contrast. No major off-resonance or  $B_1^+$  artifacts are visually apparent on the  $T_{1\rho, \text{adiab}}$  maps. In agreement with phantom and calf results, myocardial  $T_{1\rho, \text{adiab}}$  values obtained with the  $B_0$ -aSL preparation ( $\beta = 6.9$ ) are higher than those obtained with the Bal-aSL preparation ( $\beta = 5.5$ ), which in turn are higher than those obtained with  $B_1$ -aSL preparations ( $\beta = 4.4$ ). Myocardial  $T_{1\rho, \text{adiab}}$  values averaged over slices, segments, and subjects were  $194.22 \pm 24.54$  ms,  $155.59 \pm 18.09$  ms, and  $87.48 \pm 11.55$  ms for  $B_0$ -aSL, Bal-aSL, and  $B_1$ -aSL, respectively. The bullseye plots in Fig. 6 B show that

the inter-subject average  $T_{1\rho, \text{adiab}}$  values for all three aSL preparations are homogeneous across all segments. Bal-aSL and  $B_1$ -aSL bullseye plots depict lower  $T_{1\rho, \text{adiab}}$  values in the apical slice (apical vs. basal slice:  $-2.64\%$ ,  $p < 0.001$  for Bal-aSL,  $-6.62\%$ ,  $p < 0.001$  for  $B_1$ -aSL) but not for  $B_0$ -aSL ( $-0.97\%$ ,  $p = 0.12$ ).

Fig. 6 C depicts good reproducibility across the 16 AHA segments for all aSL preparations. Trends of improved precision and reproducibility were observed for  $B_0$ -aSL compared with  $B_1$ -aSL, but the differences were not significant ( $p > 0.08$ ). However,  $B_0$ -aSL yielded significantly lower inter-subject variability than  $B_1$ -aSL ( $p < 0.05$ ).

$B_0$ -aSL  $T_{1\rho, \text{adiab}}$  and RefSL  $T_{1\rho}$  maps obtained in two repetitions under different shimming conditions for a representative subject are shown in Fig. 7. RefSL preparations yield lower  $T_{1\rho}$  values than  $B_0$ -aSL (average  $T_{1\rho}$  over subjects, slices and segments =  $38.21 \pm 14.37$  ms for RefSL, compared with  $183.28 \pm 25.53$  ms for  $B_0$ -aSL, Fig. 8 A). RefSL-based  $T_{1\rho}$  maps display pronounced artifacts over large portions of the myocardium and poor reproducibility across the shimming conditions.  $B_0$ -aSL preparations, on the other hand, present comparable image quality for both cases free of visually apparent artifacts. The adiabatic  $B_0$ -aSL preparation resulted in significantly better precision compared with RefSL ( $B_0$ -aSL:  $wCV_{i,r} = 14.51 \pm 3.71\%$ , RefSL:  $wCV_{i,r} = 37.61 \pm 19.42\%$ ;  $p < 0.01$ , Fig. 8 C).

At least ten times higher reproducibility was obtained with the  $B_0$ -aSL preparation compared with the RefSL module (average  $w\bar{CV}_i = 4.64 \pm 2.18\%$  for  $B_0$ -aSL against average  $w\bar{CV}_i = 47.39 \pm 12.06\%$  for RefSL,  $p < 0.0001$ ), as shown in Fig. 8 C.

Finally, inter-subject variability was lower for the  $B_0$ -aSL preparation ( $\bar{CV} = 8.76 \pm 3.65\%$  for  $B_0$ -aSL), compared with the conventional SL ( $\bar{CV} = 51.90 \pm 15.27\%$  for RefSL,  $p < 0.0001$ ), as shown in Fig. 8 C.

A complete overview of the in vivo myocardial  $T_{1\rho, \text{adiab}}$  and  $T_{1\rho}$  values, as well as precision, reproducibility, and inter-subject variability for each healthy subject across the two cohorts, can be found in Supporting Information Tables S1, S2, S3, and S4.

### 3.4 | Patients experiments

Four of the six patients presented LGE-positive in the CMR. For two of those four patients, the mid-SAX slice intersected with the area of focal scar identified on the LGE images. Fig. 9 shows the clinical sequences as well as aSL-based  $T_{1\rho, \text{adiab}}$  maps and RefSL-based  $T_{1\rho}$  maps for the two subjects with LGE-identified scars in the mid-ventricular SAX slice.  $T_{1\rho, \text{adiab}}$  maps show visually discernable alteration in the myocardium, that spatially coincides with the areas of hyperenhancement in the LGE images. Any potential alteration in the RefSL-based  $T_{1\rho}$  maps is obfuscated by the presence of substantial artifacts.  $B_1$ -aSL yielded the best maps quality among adiabatic preparations, with no visible  $B_0$  or  $B_1^+$ -related artifacts.  $B_0$ -aSL and Bal-aSL maps were characterized by overall lower quality and presented visible artifacts across the myocardium, as shown in Supporting Information Fig. S3.

Patient 1 shows near transmural enhancement in the LGE images.  $T_{1\rho, \text{adiab}}$  in this subject shows a +47.12% elevation in the LGE-positive area compared with the remote myocardium for  $B_1$ -aSL, while RefSL-based  $T_{1\rho}$  maps show a -44.91% difference. In comparison, native  $T_1$  and  $T_2$  values for the same patient showed, respectively, +20.94% and +12.57% in the LGE-positive area. Patient 2, who showed signs of lipomatous metaplasia in bSSFP CINE images (Fig. 9), decreased relaxation times were measured for the LGE positive area, compared with remote healthy myocardium (-30.55% for  $B_1$ -aSL  $T_{1\rho, \text{adiab}}$ , -94.31% for RefSL  $T_{1\rho}$ , +8.72% for native  $T_1$ ). For both patients, normal  $T_{1\rho, \text{adiab}}$  and  $T_{1\rho}$  values were measured in the remote myocardium ( $202.18 \pm 17.79$  ms,  $169.42 \pm 13.06$  ms,  $97.98 \pm 11.35$  ms, and  $42.91 \pm 17.81$  ms for  $B_0$ -aSL, BalaSL,  $B_1$ -aSL, and RefSL, respectively). Normal  $T_{1\rho, \text{adiab}}$  and  $T_{1\rho}$  values were also measured in LGE-negative patients ( $191.32 \pm 13.53$  ms,  $148.46 \pm 12.95$  ms,  $92.35 \pm 7.29$  ms, and  $33.59 \pm 14.36$  ms for  $B_0$ -aSL, Bal-aSL,  $B_1$ -aSL, and RefSL, respectively).

## 4 | DISCUSSION

In this study, we proposed a new cardiac  $T_{1\rho, \text{adiab}}$  mapping technique based on fully aSL preparation for myocardial tissue characterization at 3T. Numerical optimization yielded aSL preparations with tuneable resilience against  $B_0$  and  $B_1^+$  inhomogeneities. Phantom and in vivo measurements demonstrated that  $T_{1\rho, \text{adiab}}$  mapping achieved more robust results than conventional  $T_{1\rho}$  mapping approaches.  $T_{1\rho, \text{adiab}}$  maps showed fewer artifacts, higher precision and reproducibility, and lower inter-subject variability. Initial data showed feasibility in patients and visual alignment of areas with altered  $T_{1\rho, \text{adiab}}$  and hyperenhancement in LGE images.

Conventional  $T_{1\rho}$  values obtained with the RefSL preparation in this study were comparable to those reported in previous studies at 3T<sup>31,32,33</sup>. However, our results show slightly lower precision for the RefSL maps than in previous studies. This difference in variability may be because previous studies only evaluated a small ROI in the anteroseptal segment of the myocardium, while in this work, an automatic segmentation of the entire myocardium was used. Significant inhomogeneities are visible in conventional RefSL maps, both in our results and in other studies<sup>31,32,33</sup>. Han et al. found that at 1.5T  $B_0$  variations over 10% of the SL field amplitude (typically  $B_1/\gamma = 500$  Hz) cause  $T_{1\rho}$  quantification errors and visible image artifacts<sup>35</sup>. At 3T, this limit is easily exceeded<sup>39</sup>. Furthermore,  $B_1^+$  inhomogeneities have a much higher impact at high fields in cardiac imaging<sup>54</sup>, thus necessitating more robust  $T_{1\rho}$  mapping techniques.

Both adiabatic and conventional  $T_{1\rho}$  maps showed lower  $T_{1\rho, \text{adiab}}$  or  $T_{1\rho}$  values in the apical slice, compared to the mid and basal slices. This effect is less evident for the  $B_0$ -aSL preparations ( $T_{1\rho, \text{adiab}}$  values comparison apical vs. mid and basal slices:  $p = 0.77$  for  $B_0$ -aSL,  $p < 0.01$  for  $B_1$ -aSL and Bal-aSL, Fig. 6). Hence, the lower  $T_{1\rho, \text{adiab}}$  and  $T_{1\rho}$  values in the apical slice may be explained with the higher contribution of  $B_0$  inhomogeneities at the apex.

Using fully aSL preparations has four major advantages. First, they yield more robust  $T_{1\rho, \text{adiab}}$  quantification in the presence of field inhomogeneities. Our results have shown

that the  $T_{1\rho, \text{adiab}}$  maps have a lower level of noise and do not present significant  $B_0$  or  $B_1^+$ -related artifacts, overcoming the limitations observed in the previous studies<sup>31,32,33</sup>.  $T_{1\rho, \text{adiab}}$  preparations also yielded higher precision, reproducibility and lower inter-subject variability. Resilience to artifacts is of particular importance for applications at high field strengths, like 3T, which have the potential advantage of increased SNR and CNR. Second, the use of amplitudemodulated HS pulses lowers the SAR demands compared to conventional continuous-wave preparations for the same duration. Wang et al. reported a SL pulse amplitude  $B_1/\gamma$  of 298 Hz<sup>33</sup>, limited by SAR constraints and comparable with our findings. Low SL pulse amplitudes result in lower measured  $T_{1\rho}$  values and further compromise the CNR and robustness to system imperfections. The aSL pulses used in this study, on the other hand, allowed us to use maximum peak power and longer preparation times, while still satisfying SAR limitations. Third,  $T_{1\rho, \text{adiab}}$  preparations eliminate the need for the initial 90° tip of the magnetization, which introduces further imperfections in the presence of  $B_1^+$  inhomogeneities<sup>42,49</sup>. Finally, conventional SL preparations are orientation-dependent<sup>55</sup>. The high anisotropy of myocardial fibers yields orientation-dependent  $T_{1\rho}$  times with conventional preparations<sup>56</sup>. Adiabatic  $T_{1\rho}$  preparations, on the other hand, have been shown to be orientation-independent<sup>55</sup>. This may further contribute to more homogeneous and reproducible  $T_{1\rho, \text{adiab}}$  maps across the myocardium.

Besides the advantages in terms of robustness given by aSL preparations, the mechanism behind  $T_{1\rho, \text{adiab}}$  relaxation is intrinsically different from conventional  $T_{1\rho}$ . Each  $T_{1\rho, \text{adiab}}$  preparation probes a wider spectrum of SL frequencies through the adiabatic sweep, compared to monofrequency conventional SL. Effective field strength and orientation vary during aSL preparations, as well as the angle between the effective field and the magnetization. On the one hand, these variations lead to relaxation rate changes throughout the preparation module, rather than sampling a uniform  $T_{1\rho}$ <sup>44,43</sup>. On the other hand, the variable transverse relaxation  $T_{2\rho}$  contribution in the rotating frame of reference results in different  $T_{1\rho}/T_{2\rho}$  ratios for any given time point. Furthermore, we observed higher  $T_{1\rho, \text{adiab}}$  times for preparations with higher  $\beta$  and, thus, a faster frequency sweep velocity. This indicates that the spectrum of relaxations rates probed during aSL varies depending on the pulse profiles. These factors may lead to a different sensitivity profile in pathological remodeling and its clinical value remains to be evaluated. An in-depth theoretical analysis of the mechanisms behind  $T_{1\rho, \text{adiab}}$  relaxation would be beneficial for the comprehension of its relationship with the underlying physiology.

In patients, the poor resilience of RefSL preparations to system imperfections significantly compromised the map quality. Artifacts in the area around the coronary sinus, as well as the lateral wall, appeared in all cases, preventing the unambiguous identification of focal alteration. Compared to healthy subjects, image artifacts were substantially more pronounced in the patient cohort. This likely stemmed from lower  $B_1^+$  shim quality in the clinical setting. aSL-based preparations, in particular when tuned for  $B_1^+$ -resilience, yielded good map quality, comparable to the healthy subject cohort. This indicates fair resilience to system imperfections in clinical use.

Cardiac  $T_{1\rho, \text{adiab}}$  maps showed visible focal alteration that spatially coincided with areas of hyperenhancement in the LGE images. This is in line with previous studies indicating sensitivity to a range of diseases. Wang et al. found a +24%  $T_{1\rho}$  elevation for hypertrophic cardiomyopathy patients with diffuse fibrosis<sup>33</sup>. At 1.5T, van Oorschot et al. measured +52%  $T_{1\rho}$  elevation in infarcted myocardium of patients suffering from ischemic heart disease<sup>?</sup> and +46% in a second ischemic cohort<sup>27</sup>. Furthermore, Bustin et al. have found a +40% elevation in infarcted myocardium of LGE-positive patients<sup>29</sup>. Our preliminary results indicate that fully adiabatic  $T_{1\rho}$  mapping can potentially yield more robust quantification than conventional continuous-wave SL in clinical use at high fields. However, clinical sensitivity of  $T_{1\rho, \text{adiab}}$  mapping may differ from conventional continuous wave  $T_{1\rho}$  mapping due to the mechanistic differences and among different adiabatic preparations due to differences in the effective and fictitious fields. Consequently, larger dedicated cohorts of healthy controls and a targeted patient population are warranted to determine clinical sensitivity and potential cut-off values for the differentiation of healthy and infarcted myocardium.

Pulse design optimization was the key to achieving the desired resilience against  $B_0$  and  $B_1^+$  inhomogeneities. The HS pulse shape was chosen specifically for its enhanced resilience to  $B_0$  inhomogeneities, superior to TANH/TAN pulses, as previously reported<sup>39</sup>. First, we observed that shorter aSL pulses (4HS-aSL and 8HS-aSL) performed worse than the longer one 2HS-aSL, despite allowing for complete MLEV compensation. Longer HS pulses are thus preferred for  $T_{1\rho, \text{adiab}}$  preparations. Second, we found that the optimal HS pulse shape varies significantly under different  $B_0$  and  $B_1^+$  conditions. Bloch simulations were in very good agreement with the experimental data acquired in both the phantoms and the calf muscle. Our in vivo results show that  $B_0$ -aSL preparations achieve better precision and inter-subject variability than Bal-aSL and  $B_1$ -aSL in healthy subjects. However,  $B_1$ -aSL has proven most robust in the clinical set-up where  $B_1$ -shim quality was reduced.

Increased  $wCV_{r,i}$ ,  $w\bar{C}V_i$ , and  $\bar{C}V$  values were observed in the basal and mid-inferolateral segment, as well as the apical lateral segment for  $B_1$ -aSL preparations (see Fig. 8). These values were reflected in the  $B_1$ -aSL  $T_{1\rho, \text{adiab}}$  maps, which, for some subjects, presented residual  $B_0$  artifacts in the same segments (Fig. 7). These effects were not observed for  $B_0$ -aSL and Bal-aSL maps. Thus, depending on the application and the technical characteristics of the scanner either of the optimized preparations may be most suitable for robust  $T_{1\rho, \text{adiab}}$  quantification in the clinic. Adiabatic pulses that were previously used for other cardiac MRI applications were found to be closest to those used for  $B_1$ -aSL preparations ( $\beta = 4.8$ ,  $f_{\text{max}} = 215 \text{ Hz}$ <sup>40</sup>). These pulses may be particularly warranted on systems where  $B_1$  quality is the main concern, such as systems with a single transmit channel or a lack of advanced shim modes. On other systems,  $B_0$ -aSL and Bal-aSL preparations may be preferred for the observed increase in precision and reproducibility.

In our study, patient scans showed pronounced cardiac and respiratory motion, despite cardiac triggering and breathholding. Residual motion due to heart rate variability and poor breath-holding capacity in patients rendered retrospective image registration necessary to achieve satisfactory map quality in the final  $T_{1\rho, \text{adiab}}$  and  $T_{1\rho}$  maps. Recently, specific

attention has been dedicated on the development of accelerated, free-breathing, whole-heart  $T_{1\rho}$  mapping sequences to facilitate its clinical implementation<sup>57,28,58</sup>. Furthermore, several motion correction approaches have been proposed to improve the quality of reconstructed  $T_{1\rho}$  maps and mitigate the contribution of motion<sup>26,29</sup>. These efforts are key to enabling the widespread use of quantitative parametric mapping sequences in clinical practice. Our aSL preparations are fully compatible with these sequence designs and reconstruction approaches and could, in the future, be integrated into accelerated and motion-corrected  $T_{1\rho}$  mapping sequences. This may be particularly helpful to facilitate testing of the proposed  $T_{1\rho, \text{adiab}}$  mapping in large, relevant patient cohorts in order to demonstrate its clinical value.

## 5 | CONCLUSIONS

In this work,  $T_{1\rho, \text{adiab}}$  mapping was proposed as an alternative to conventional  $T_{1\rho}$  mapping to enable its application in the human myocardium at 3T. Our results show that adiabatic spin-lock preparations enable more robust mapping in the presence of  $B_0$  and  $B_1^+$  inhomogeneities while satisfying SAR limitations. Adiabatic preparation modules yielded quantification with high precision and reproducibility in healthy subjects. In patients, aSL-based  $T_{1\rho, \text{adiab}}$  maps depicted focal alterations in agreement with the reference LGE scans. Thus,  $T_{1\rho}$  mapping can be a promising candidate for reproducible myocardial tissue characterization and bears potential as a contrast-free imaging biomarker for scar and fibrosis.

## Supplementary Material

Refer to Web version on PubMed Central for supplementary material.

## ACKNOWLEDGMENTS

We would like to thank Paul de Bruin, Ece Ercan, and David Higgins for their help in facilitating the patient scans. We also thank Joke Smink for his valuable input regarding the pulse sequence development.

## Funding Information

This work was supported by the 4TU federation, a NWO Start-up grant STU.019.024, and ZonMW Off-Road 04510011910073.

## REFERENCES

1. Kim Raymond J, Chen Enn Ling, Lima João A.C., Judd Robert M.. Myocardial Gd-DTPA Kinetics Determine MRI Contrast Enhancement and Reflect the Extent and Severity of Myocardial Injury After Acute Reperfused Infarction. *Circulation*. 1996;94:3318–3326. [PubMed: 8989146]
2. Kim Raymond J, Wu Edwin, Rafael Allen, et al. The Use of Contrast-Enhanced Magnetic Resonance Imaging to Identify Reversible Myocardial Dysfunction. *New England Journal of Medicine*. 2000;343(20):1445–1453. [PubMed: 11078769]
3. Kim Han W, Farzaneh-Far Afshin, Kim Raymond J.. Cardiovascular Magnetic Resonance in Patients With Myocardial Infarction. Current and Emerging Applications. *Journal of the American College of Cardiology*. 2009;55:1–16. [PubMed: 20117357]
4. Rajiah Prabhakar, Desai Milind Y., Kwon Deborah, Flamm Scott D.. MR imaging of myocardial infarction. *Radiographics*. 2013;33:1383–1412. [PubMed: 24025931]
5. Abdel-Aty Hassan, Zagrosek Anja, Schulz-Menger Jeanette, et al. Delayed enhancement and T2-weighted cardiovascular magnetic resonance imaging differentiate acute from chronic myocardial infarction. *Circulation*. 2004;109:2411–2416. [PubMed: 15123531]

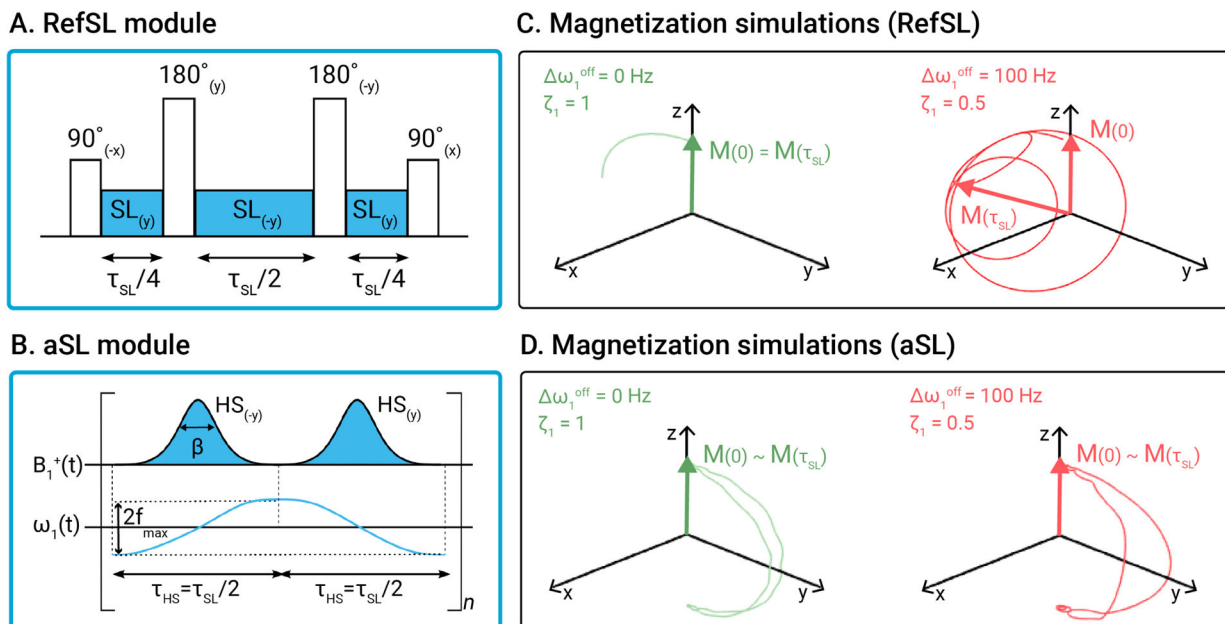
6. Ledneva Elena, Karie Svetlana, Launay-Vacher Vincent, Janus Nicolas, Deray Gilbert. Renal safety of gadolinium- Based contrast media in patients with chronic renal insufficiency. *Radiology*. 2009;250:618–628. [PubMed: 19244037]
7. Kanda Tomonori, Ishii Kazunari, Kawaguchi Hiroki, Kitajima Kazuhiro, Takenaka Daisuke. High signal intensity in the dentate nucleus and globus pallidus on unenhanced T1-weighted MR images: Relationship with increasing cumulative dose of a gadoliniumbased contrast material. *Radiology*. 2014;270:834–841. [PubMed: 24475844]
8. Ismail Tevfik F, Strugnell Wendy, Coletti Chiara, et al. Cardiac MR: From Theory to Practice. *Frontiers in Cardiovascular Medicine*. 2022;0:137.
9. Dall' Armellina Erica, Piechnik Stefan K., Ferreira Vanessa M., et al. Cardiovascular magnetic resonance by non contrast T1-mapping allows assessment of severity of injury in acute myocardial infarction. *Journal of Cardiovascular Magnetic Resonance*. 2012;14:1–13. [PubMed: 22226320]
10. Carrick David, Haig Caroline, Rauhalampi Sam, et al. Prognostic significance of infarct core pathology revealed by quantitative noncontrast in comparison with contrast cardiac magnetic resonance imaging in reperfused ST-elevation myocardial infarction survivors. *European Heart Journal*. 2016;37:1044–1059. [PubMed: 26261290]
11. Nakamori Shiro, Alakbarli Javid, Bellm Steven, et al. Native T1 value in the remote myocardium is independently associated with left ventricular dysfunction in patients with prior myocardial infarction. *Journal of Magnetic Resonance Imaging*. 2017;46:1073–1081. [PubMed: 28152237]
12. Ugander Martin, Bagi Paul S., Oki Abiola J., et al. Myocardial Edema as Detected by Pre-Contrast T1 and T2 CMR Delineates Area at Risk Associated With Acute Myocardial Infarction. *JACC: Cardiovascular Imaging*. 2012;5:596–603. [PubMed: 22698528]
13. Stoffers Rutger H, Madden Marie, Shahid Mohammed, et al. Assessment of myocardial injury after reperfused infarction by T1 $\rho$  cardiovascular magnetic resonance. *Journal of Cardiovascular Magnetic Resonance*. 2017;19:1–10. [PubMed: 28081721]
14. Aherne Emily, Chow Kelvin, Carr James. Cardiac T1 mapping: Techniques and applications. *Journal of Magnetic Resonance Imaging*. 2020;51(5):1336–1356. [PubMed: 31334899]
15. Martino AF, Damadian R. Improved discrimination of normal and malignant tissue using <sup>1</sup>H NMR relaxation time measurements at 2.18 MHz.. *Physiological Chemistry and Physics and Medical NMR*. 1984;16:49–55. [PubMed: 6541347]
16. Sepponen Raimo E, Pohjonen Jaakko A, Sipponen Jorma T, Tanttu Jukka I. A method for T1  $\rho$  imaging. *Journal of computer assisted tomography*. 1985;9:1007–1011. [PubMed: 4056129]
17. Muthupillai Raja, Flamm Scott D., Wilson James M., Pettigrew Roderic I., Thomas Dixon W.. Acute myocardial infarction: Tissue characterization with T1  $\rho$ -weighted MR imaging - Initial experience. *Radiology*. 2004;232:606–610. [PubMed: 15215547]
18. Huber Steffen, Muthupillai Raja, Lambert Brenda, Pereyra Mercedes, Napoli Alicia, Flamm Scott D.. Tissue characterization of myocardial infarction using T1 $\rho$ : Influence of contrast dose and time of imaging after contrast administration. *Journal of Magnetic Resonance Imaging*. 2006;24:1040–1046. [PubMed: 16972231]
19. Witschey Walter RT, Pilla James J, Ferrari Giovanni, et al. Rotating frame spin lattice relaxation in a swine model of chronic, left ventricular myocardial infarction. *Magnetic Resonance in Medicine*. 2010;64:1453–1460. [PubMed: 20677236]
20. Witschey Walter Rt, Zsido Gerald A., Kevin Koomalsingh, et al. In vivo chronic myocardial infarction characterization by spin locked cardiovascular magnetic resonance. *Journal of Cardiovascular Magnetic Resonance*. 2012;14:1–9. [PubMed: 22226320]
21. Musthafa Haja Sherief N, Dragneva Galina, Lottonen Line, et al. Longitudinal rotating frame relaxation time measurements in infarcted mouse myocardium in vivo. *Magnetic Resonance in Medicine*. 2013;69:1389–1395. [PubMed: 22736543]
22. Gram Maximilian, Gensler Daniel, Winter Patrick, et al. Fast myocardial T1 $\rho$  mapping in mice using *k*-space weighted image contrast and a Bloch simulation-optimized radial sampling pattern. *Magnetic Resonance Materials in Physics, Biology and Medicine*. 2022;35:325–340.
23. Maximilian Gram, Daniel Gensler, Petra Albertova, et al. Quantification correction for free-breathing myocardial T1 $\rho$  mapping in mice using a recursively derived description of a T1 $\rho$

- \* relaxation pathway. *Journal of Cardiovascular Magnetic Resonance*. 2022;24:1–16. [PubMed: 34986851]
24. Zhang Yu, Zeng Wen, Chen Wei, et al. MR extracellular volume mapping and non-contrast T1 $\rho$  mapping allow early detection of myocardial fibrosis in diabetic monkeys. *European Radiology*. 2019;29:3006–3016. [PubMed: 30643944]
  25. Oorschot Joep W.M., Aidi Hamza El, Jansen Lorkeers Sanne J., et al. Endogenous assessment of chronic myocardial infarction with T(1 $\rho$ )-mapping in patients. *Journal of cardiovascular magnetic resonance : official journal of the Society for Cardiovascular Magnetic Resonance*. 2014;16:104. [PubMed: 25526973]
  26. Berisha Sebastian, Han Joyce, Shahid Mohammed, Han Yuchi, Witschey Walter R.T.. Measurement of Myocardial T1 $\rho$  with a Motion Corrected, Parametric Mapping Sequence in Humans. *PLOS ONE*. 2016;11:e0151144. [PubMed: 27003184]
  27. Oorschot Joep W.M. Van, Visser Fredy, Eikendal Anouk L.M., et al. Single Breath-Hold T1 $\rho$  -Mapping of the Heart for Endogenous Assessment of Myocardial Fibrosis. *Investigative Radiology*. 2016;51:505–512. [PubMed: 26895195]
  28. Haikun Qi, Aurelien Bustin, Thomas Kuestner, et al. Respiratory motion-compensated high-resolution 3D whole-heart T1 $\rho$  mapping. *Journal of Cardiovascular Magnetic Resonance*. 2020;22:1–13. [PubMed: 31898543]
  29. Bustin Aurélien Toupin Solemn, Soumaya Sridi, et al. Endogenous assessment of myocardial injury with single-shot model-based non-rigid motion-corrected T1 rho mapping. *Journal of Cardiovascular Magnetic Resonance*. 2021;23:1–14. [PubMed: 33390185]
  30. Thompson Elizabeth W., Iyer Srikant Kamesh, Solomon Michael P., et al. Endogenous T1 $\rho$  cardiovascular magnetic resonance in hypertrophic cardiomyopathy. *Journal of Cardiovascular Magnetic Resonance*. 2021;23:1–9. [PubMed: 33390185]
  31. Wang Chunhua, Zheng Jie, Sun Jiayu, et al. Endogenous contrast T1rho cardiac magnetic resonance for myocardial fibrosis in hypertrophic cardiomyopathy patients. *Journal of Cardiology*. 2015;66:520–526. [PubMed: 25981868]
  32. Lin Wang, Jing Yuan, Zhang Shi Jun, et al. Myocardial T1rho mapping of patients with end-stage renal disease and its comparison with T1 mapping and T2 mapping: A feasibility and reproducibility study. *Journal of Magnetic Resonance Imaging*. 2016;44:723–731. [PubMed: 26889749]
  33. Wang Keyan, Zhang Wenbo, Li Shuman, et al. Noncontrast T1 $\rho$  dispersion imaging is sensitive to diffuse fibrosis: A cardiovascular magnetic resonance study at 3T in hypertrophic cardiomyopathy. *Magnetic Resonance Imaging*. 2022;91:1–8. [PubMed: 35525524]
  34. Witschey Walter RT, Borthakur Arijitt, Elliott Mark A., et al. Artifacts in T1 $\rho$  -weighted imaging: Compensation for B1 and B0 field imperfections. *Journal of Magnetic Resonance*. 2007;186:75–85. [PubMed: 17291799]
  35. Han Qiao, Han Yuchi, Gorman Robert C, Witschey Walter R. The influence of static and RF field heterogeneity on T1rho cardiovascular MRI. *Journal of Cardiovascular Magnetic Resonance* 2014 16:1. 2014;16:1–3
  36. Charagundla Sridhar R., Borthakur Arijitt, Leigh John S., Reddy Ravinder. Artifacts in T1 $\rho$ -weighted imaging: correction with a self-compensating spin-locking pulse. *Journal of Magnetic Resonance*. 2003;162:113–121. [PubMed: 12762988]
  37. Gram Maximilian, Seethaler Michael, Gensler Daniel, Oberberger Johannes, Jakob Peter M., Nordbeck Peter. Balanced spin-lock preparation for B1-insensitive and B0-insensitive quantification of the rotating frame relaxation time T1 $\rho$ . *Magnetic Resonance in Medicine*. 2021;85:2771–2780. [PubMed: 33166009]
  38. Garwood Michael, Delabarre Lance. The Return of the Frequency Sweep: Designing Adiabatic Pulses for Contemporary NMR. *Journal of Magnetic Resonance*. 2001;153:155–177. [PubMed: 11740891]
  39. Kellman Peter, Hansen Michael S.. T1-mapping in the heart: Accuracy and precision. *Journal of Cardiovascular Magnetic Resonance*. 2014;16:1–20. [PubMed: 24387349]



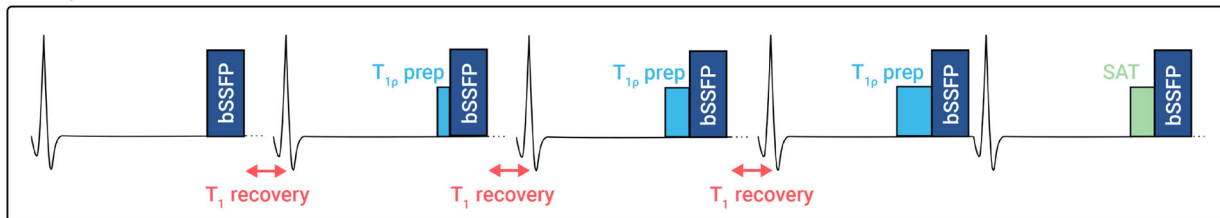
40. Nezafat Reza, Stuber Matthias, Ouwerkerk Ronald, Gharib Ahmed M., Desai Milind Y., Pettigrew Roderic I. B1-insensitive T2 preparation for improved coronary magnetic resonance angiography at 3 T. *Magnetic Resonance in Medicine*. 2006;55:858–864. [PubMed: 16538606]
41. Michaeli Shalom, Sorce Dennis J., Springer Charles S., Ugurbil Kamil, Garwood Michael. T1 $\rho$  MRI contrast in the human brain: Modulation of the longitudinal rotating frame relaxation shutter-speed during an adiabatic RF pulse. *Journal of Magnetic Resonance*. 2006;181:135–147 [PubMed: 16675277]
42. Mangia Silvia, Liimatainen Timo, Garwood Michael, Michaeli Shalom. Rotating frame relaxation during adiabatic pulses vs. conventional spin lock: simulations and experimental results at 4 T. *Magnetic Resonance Imaging*. 2009;27:1074–1087. [PubMed: 19559559]
43. Sorce Dennis J, Michaeli Shalom, Garwood Michael. Relaxation During Adiabatic Radiofrequency Pulses. *Current Analytical Chemistry*. 2007;3:239–251.
44. Michaeli Shalom, Sorce Dennis J., Garwood Michael. T2 $\rho$  and T1 $\rho$  Adiabatic Relaxations and Contrasts. *Current Analytical Chemistry*. 2008;4:8–25.
45. Jerban Saeed, Ma Yajun, Kasibhatla Akhil, et al. Ultrashort echo time adiabatic T1 $\rho$  (UTE-Adiab-T1 $\rho$ ) is sensitive to human cadaveric knee joint deformation induced by mechanical loading and unloading. *Magnetic Resonance Imaging*. 2021;80:98–105. [PubMed: 33945858]
46. Okuaki Tomoyuki, Takayama Yukihisa, Nishie Akihiro, et al. T1 $\rho$  mapping improvement using stretched-type adiabatic locking pulses for assessment of human liver function at 3T. *Magnetic Resonance Imaging*. 2017;40:17–23. [PubMed: 28363761]
47. Levitt Malcolm H. Composite pulses. *Progress in Nuclear Magnetic Resonance Spectroscopy*. 1986;18:61–122.
48. Weingärtner Sebastian, Zimmer Fabian, Metzger Gregory J., Ugurbil Kâmil, Moortele Pierre Francois Van, Akçakaya Mehmet. Motion-robust cardiac mapping at 3T using interleaved bloch-siegert shifts. *Magnetic Resonance in Medicine*. 2017;78:670–677. [PubMed: 27599782]
49. Akçakaya Mehmet, Basha Tamer A., Weingärtner Sebastian, Roujol Sébastien, Berg Sophie, Nezafat Reza. Improved quantitative myocardial T2 mapping: Impact of the fitting model. *Magnetic Resonance in Medicine*. 2015;74:93–105. [PubMed: 25103908]
50. Captur Gabriella, Gatehouse Peter, Keenan Kathryn E., et al. A medical device-grade T1 and ECV phantom for global T1 mapping quality assurance - the T1 Mapping and ECV Standardization in cardiovascular magnetic resonance (TIMES) program. *Journal of Cardiovascular Magnetic Resonance*. 2016;18:1–20. [PubMed: 26732096]
51. Weingärtner Sebastian, Desmond Kimberly L., Obuchowski Nancy A., et al. Development, validation, qualification, and dissemination of quantitative MR methods: Overview and recommendations by the ISMRM quantitative MR study group. *Magnetic Resonance in Medicine*. 2022;87:1184–1206. [PubMed: 34825741]
52. Isensee Fabian, Jaeger Paul F., Kohl Simon A.A., Petersen Jens, Maier-Hein Klaus H.. nnU-Net: a self-configuring method for deep learning-based biomedical image segmentation. *Nature Methods* 2020 18:2. 2020;18:203–211.
53. Zhao Yidong, Yang Changchun, Schweidtmann Artur, Tao Qian. Efficient Bayesian uncertainty estimation for nnU-Net. *International Conference on Medical Image Computing and Computer Assisted Intervention*. 2022;
54. Weingärtner Sebastian, Zimmer Fabian, Metzger Gregory J., Ugurbil Kâmil, Moortele Pierre Francois Van, Akçakaya Mehmet. Motion-robust cardiac mapping at 3T using interleaved bloch-siegert shifts. *Magnetic Resonance in Medicine*. 2017;78:670–677. [PubMed: 27599782]
55. Hänninen Nina, Rautiainen Jari, Rieppo Lassi, Saarakkala Simo, Nissi Mikko Johannes. Orientation anisotropy of quantitative MRI relaxation parameters in ordered tissue. *Scientific Reports* 2017 7:1. 2017;7:1–11.
56. Aliotta Eric, Moulin Kévin, Magrath Patrick, Ennis Daniel B.. Quantifying precision in cardiac diffusion tensor imaging with second-order motion-compensated convex optimized diffusion encoding. *Magnetic Resonance in Medicine*. 2018;80:1074–1087. [PubMed: 29427349]
57. Iyer Srikant Kamesh, Moon Brianna, Hwuang Eileen, et al. Accelerated free-breathing 3D T1 $\rho$  cardiovascular magnetic resonance using multicoil compressed sensing. *Journal of Cardiovascular Magnetic Resonance*. 2019;21:1–11. [PubMed: 30612574]

58. Velasco Carlos, Cruz Gastão, Lavin Begoña, et al. Simultaneous T1, T2, and T1 $\rho$  cardiac magnetic resonance fingerprinting for contrast agent-free myocardial tissue characterization. *Magnetic Resonance in Medicine*. 2022;87:1992–2002. [PubMed: 34799854]
59. Tao Qian, van der Tol Pieternel, Berendsen Floris F, et al. Robust motion correction for myocardial T1 and extracellular volume mapping by principle component analysis-based groupwise image registration *Journal of Magnetic Resonance Imaging*. 2018;47:1397–1405. [PubMed: 28960659]
60. Captur Gabriella, Gatehouse Peter, Keenan Kathryn E, et al. A medical device-grade T1 and ECV phantom for global T1 mapping quality assurance — the T1 Mapping and ECV Standardization in cardiovascular magnetic resonance (TIMES) program *Journal of cardiovascular magnetic resonance*. 2016;18:1–20. [PubMed: 26732096]
61. Ogg Robert J, Kingsley Peter B, and Taylor June S. WET, a T1- and B1-insensitive water-suppression method for in vivo localized <sup>1</sup>H NMR spectroscopy *Journal of Magnetic Resonance, Series B*. 1994;104:1–10. [PubMed: 8025810]
62. Schär Michael, Vonken Evert-Jan, and Stuber Matthias. Simultaneous B0- and B1+-Map acquisition for fast localized shim, frequency, and RF power determination in the heart at 3T *Magnetic Resonance in Medicine* 2010;63:419–426. [PubMed: 20099330]
63. Noeske Ralph, Seifert Frank, Rhein Karl-Heinz, and Rinneberg Herbert. Human cardiac imaging at 3T using phased array coils *Magnetic Resonance in Medicine* 2000; 44:978–982. [PubMed: 11108638]

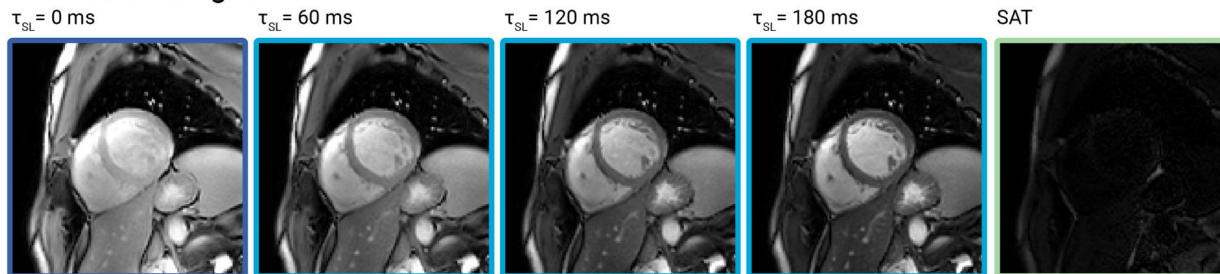


**Figure 1.**

(A) Conventional SL pulse (RefSL) and (B) adiabatic SL pulse (aSL), with corresponding amplitude and frequency modulation functions. Magnetization trajectories for the RefSL (C) and aSL (D) modules, simulated under ideal conditions (off-resonance  $\Delta\omega_1^{\text{off}} = 0$  Hz, relative  $B_1^+\zeta_1 = 1$ ) and in presence of moderate  $B_0$  and  $B_1^+$  inhomogeneities ( $\Delta\omega_1^{\text{off}} = 100$  Hz,  $\zeta_1 = 0.5$ ). The parameters used for aSL were:  $\tau_{HS} = 30$  ms,  $\beta = 5.5$ ,  $f_{\text{max}} = 350$  Hz,  $B_1^{\text{max}} = 13.5 \mu\text{T}$ . Major deviations from the idealized case are observed for the RefSL preparation in the presence of inhomogeneities, while the aSL preparation produces similar results in both cases.

A.  $T_{1\rho}$  mapping sequence

## B. Baseline images

**Figure 2.**

(A)  $T_{1\rho}$  mapping sequence diagram with (B) corresponding baseline images from a representative healthy subject. Five images are acquired, one without preparation, three with different  $T_{1\rho, \text{adiab}}$  preparations ( $\tau_{\text{SL}} = 60, 120, 180$  ms), and one with saturation preparation, to allow for accurate mapping of the induced  $T_{1\rho}$  relaxation.

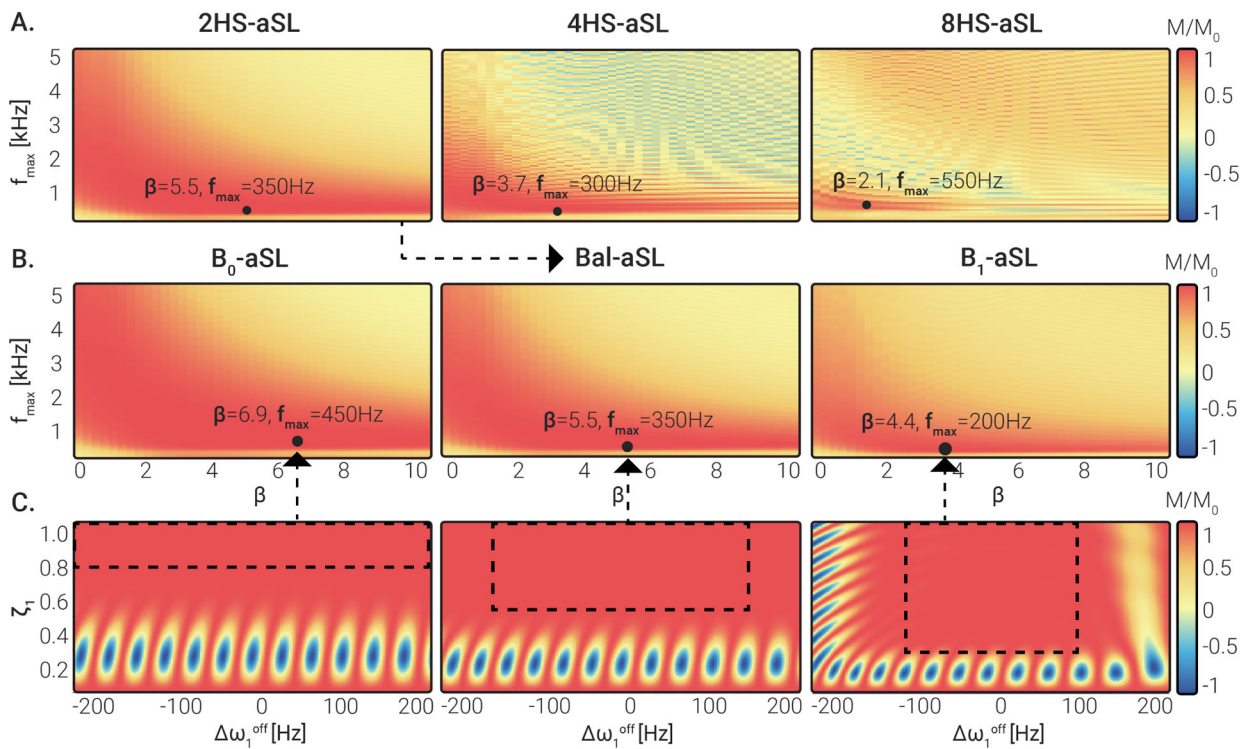


**Figure 3.**

(A) Simulated preparation efficiency for 2HS-aSL, 4HS-aSL and 8HS-aSL preparations, obtained by concatenating 2 ( $\tau_{HS} = 30$  ms), 4 ( $\tau_{HS} = 15$  ms), or 8 ( $\tau_{HS} = 7.5$  ms) HS pulses, respectively.  $M_z/M_0$  was averaged over a design window covering  $\Delta\omega_1^{\text{off}} \in \{-150, -149, \dots, +150\}$  Hz and  $\zeta_1 \in \{0.50, 0.49, \dots, 1.00\}$ . Combinations of  $\beta$  and  $f_{\max}$  yielding the highest efficiency are indicated for each module by a black dot. (B) Simulated preparation efficiency for 2HS-aSL, using three different design regions:  $B_0$ -aSL, Bal-aSL and  $B_1$ -aSL. Black dots mark the combination of  $\beta$  and  $f_{\max}$  yielding the highest preparation efficiency. The highest efficiency was obtained for low  $f_{\max}$  amplitudes and intermediate  $\beta$ . (C) Simulated preparation efficiency obtained for the optimal  $\beta$  and  $f_{\max}$  combination identified in (B) for various  $\Delta\omega_1^{\text{off}}$  and  $\zeta_1$ . Dashed black boxes represent the design region considered for each pulse in (B).

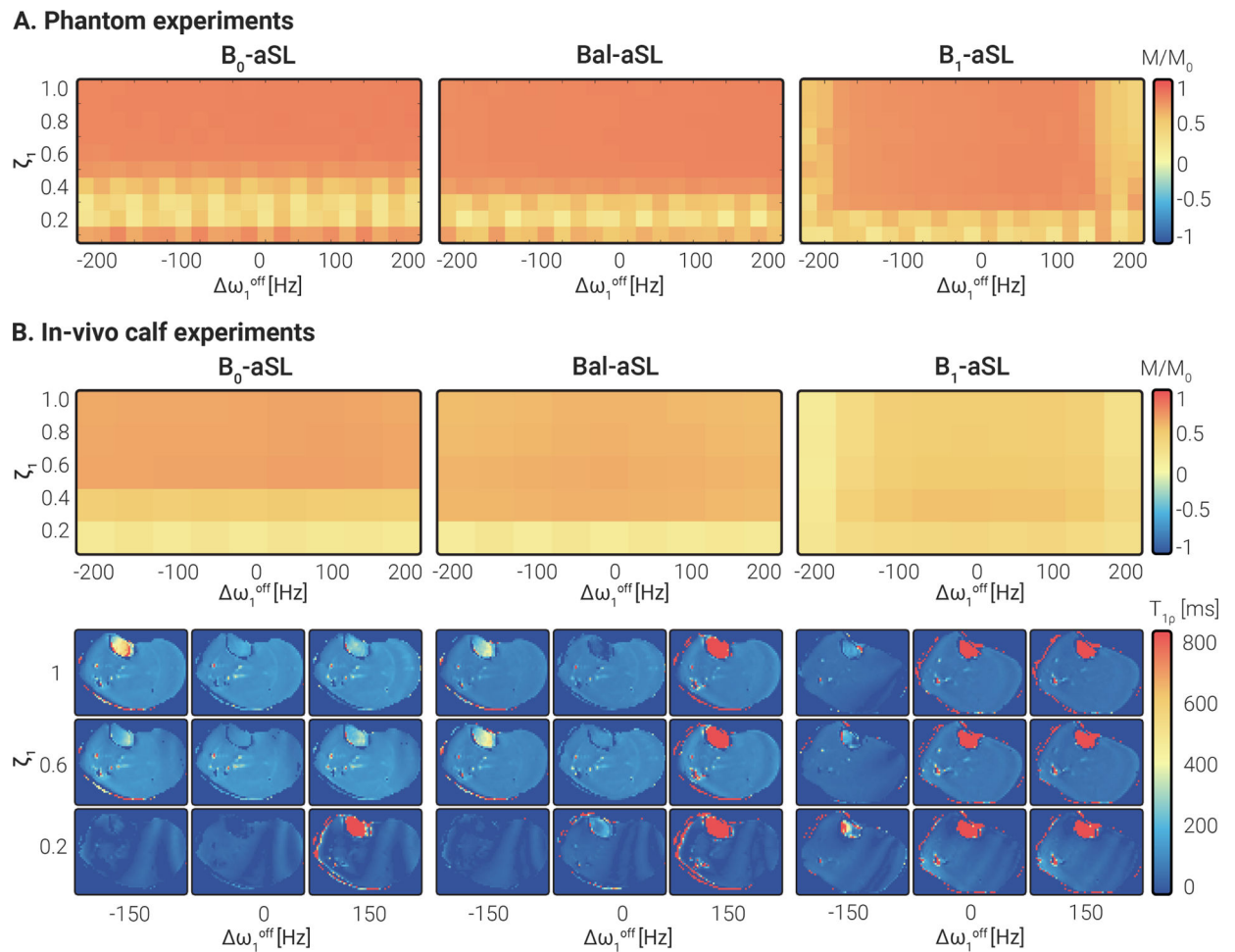


**Figure 4.**

(A) Experimental preparation efficiency measured in phantoms for a range of  $\Delta\omega_1^{\text{off}}$  and  $\zeta_1$  with three aSL preparations. Experimental results were in agreement with simulations in Fig. 3 C, minus a scaling factor given by relaxation, which was ignored in simulations. (B) Adiabatic preparations efficiency was measured in vivo on a healthy subject's calf muscle for the same range of  $\Delta\omega_1^{\text{off}}$  and  $\zeta_1$ . Overall, the results were in good agreement with the phantom experiments (A) and the numerical simulations (Fig. 3 C). Representative calf  $T_{1\rho, \text{adiab}}$  maps for different values of  $\Delta\omega_1^{\text{off}}$  and  $\zeta_1$  illustrate the variation in image artifacts.

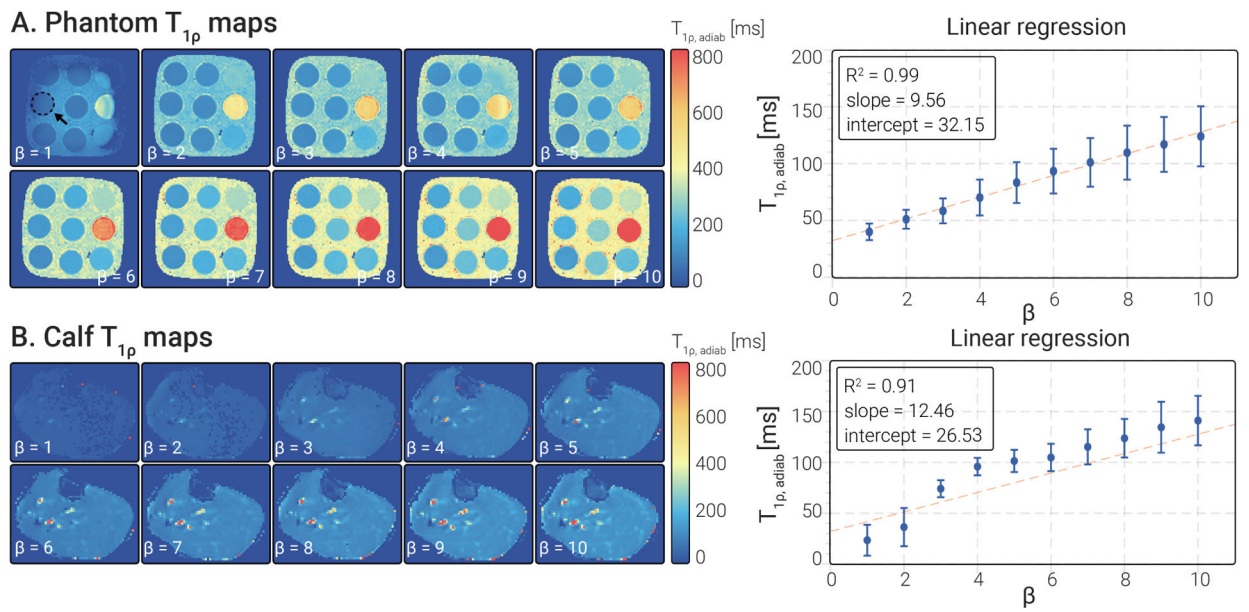
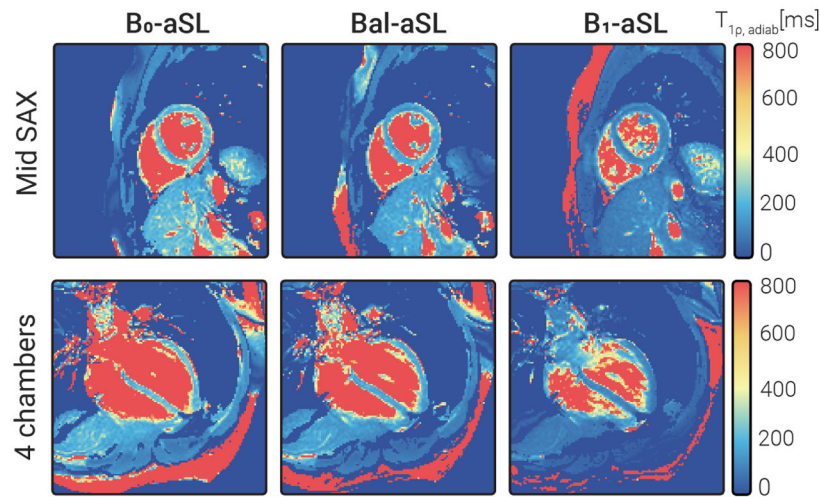


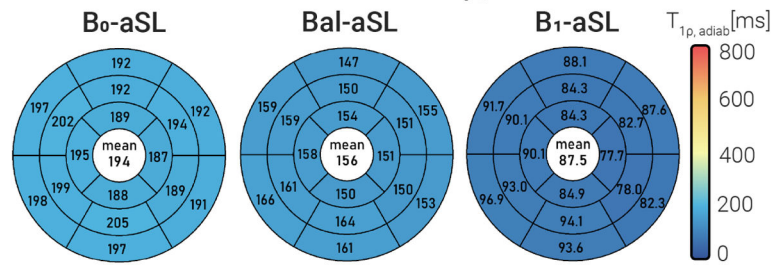
**Figure 5.**

(A) Phantom and (B) calf  $T_{1\rho, \text{adiab}}$  maps were obtained for various  $\beta$  and constant  $f_{\text{max}} = 350$  Hz. Linear regression analysis results showed that both phantoms and calf present a linear relationship between the pulse  $\beta$  and the measured  $T_{1\rho, \text{adiab}}$  values.

### A. Healthy subjects: $T_{1\rho, \text{adiab}}$ maps



### B. Healthy subjects: average $T_{1\rho, \text{adiab}}$



### C. Healthy subjects: reproducibility (with patient repositioning)

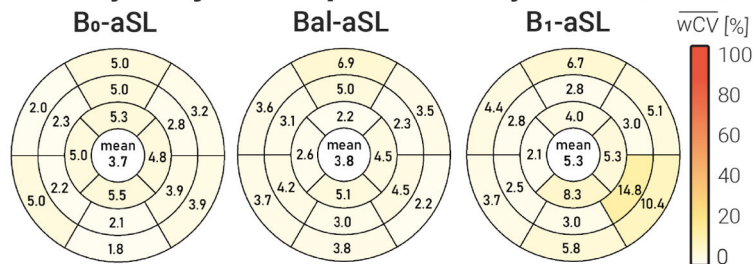


**Figure 6.**

(A) Mid SAX and 4ch  $T_{1\rho, \text{adiab}}$  maps obtained with  $B_0$ -aSL, Bal-aSL, and  $B_1$ -aSL preparations in a representative healthy subject of the first cohort.  $T_{1\rho, \text{adiab}}$  maps achieved good visual map quality, with a homogeneous myocardium and clear delineation against the blood pool across all acquired slices. (B) Bullseye plots showing the  $T_{1\rho, \text{adiab}}$  values, averaged over all subjects and repetitions, for 16 AHA myocardial segments.  $T_{1\rho, \text{adiab}}$  values are homogeneous across the 16 segments for all preparations. Average  $T_{1\rho, \text{adiab}}$  increase with increasing beta  $\beta$ . (C) Bullseye plots report the average reproducibility ( $w\bar{C}V$ ) coefficients, measured over 2 acquisitions interleaved by subject repositioning, for aSL-prepared maps in 16 AHA myocardial segments. Global average values are reported at the center of each bullseye plot.



A mild improvement in reproducibility is observed for  $B_0$ -aSL and Bal-aSL preparations, compared to  $B_1$ -aSL, but the difference was not statistically significant ( $p > 0.05$ ).

Author Manuscript

Author Manuscript

Author Manuscript

Author Manuscript

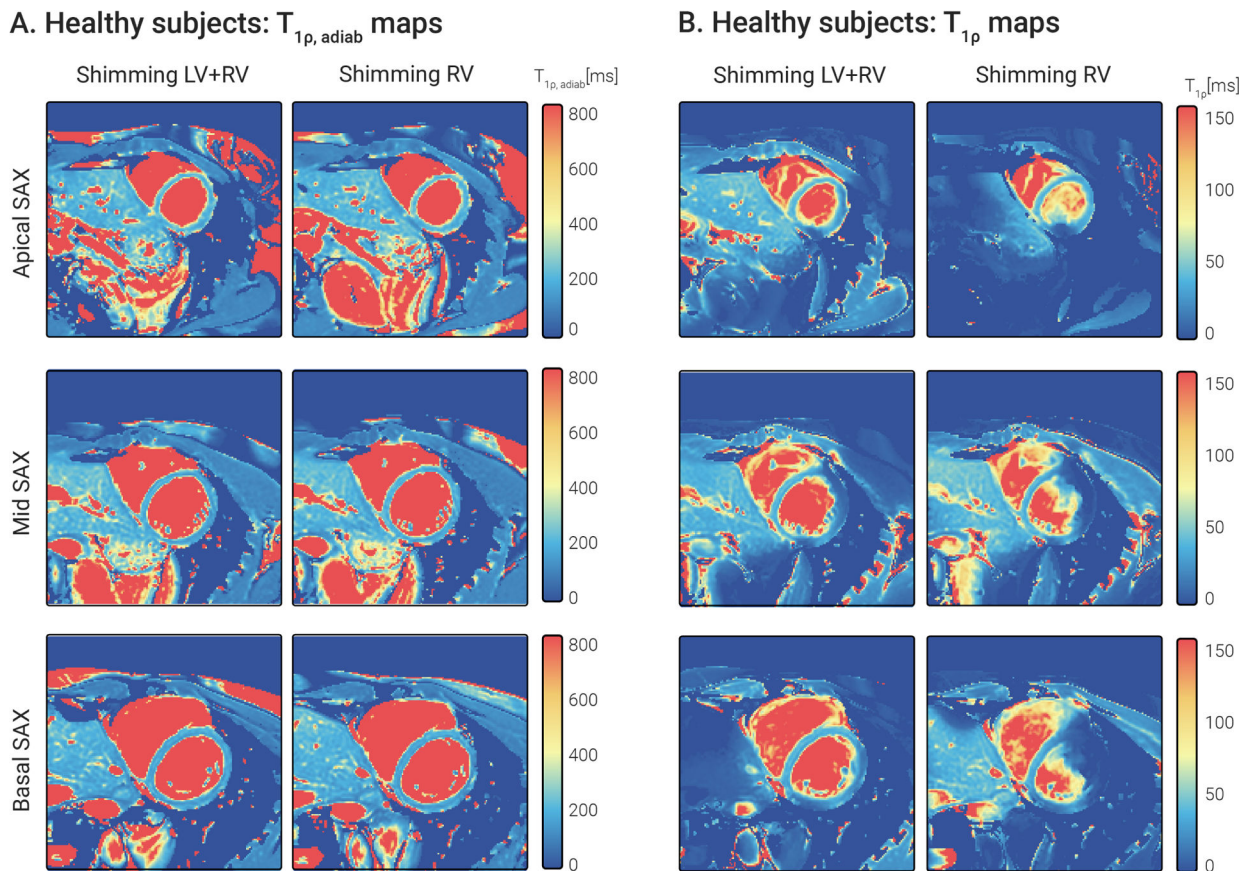
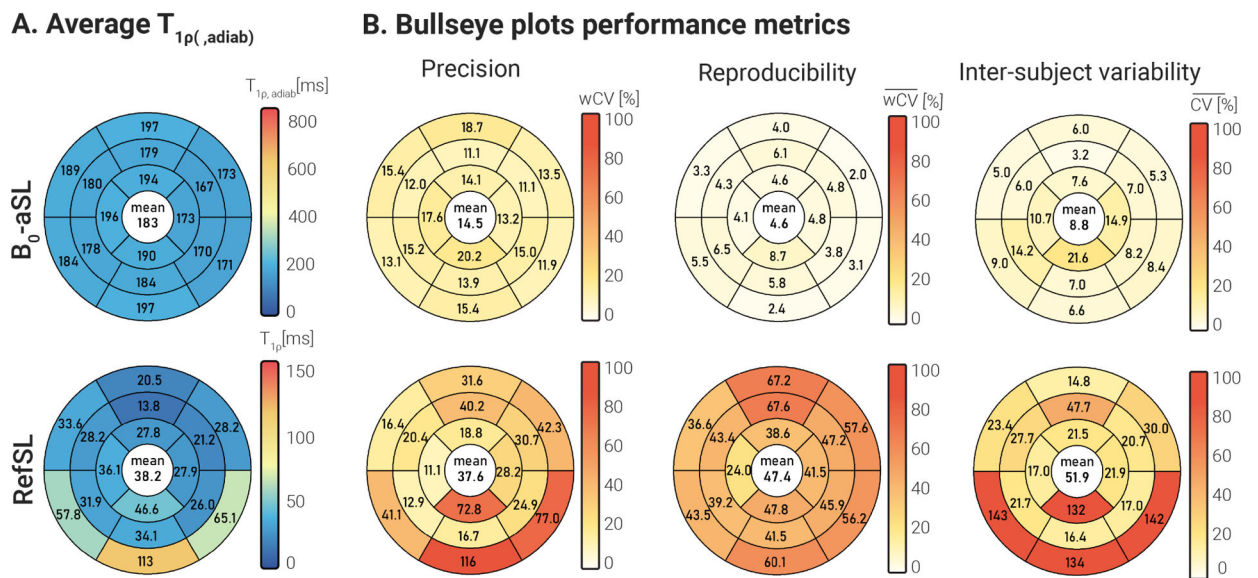


**Figure 7.**

Apical, mid, and basal SAX (A)  $B_0$ -aSL-prepared  $T_{1\rho, \text{adiab}}$  maps and (B) RefSL-prepared  $T_{1\rho}$  maps in a representative healthy subject. Two repetitions of each slice and preparation were acquired with different shim volumes: one covering the entire heart, the other covering only the right ventricle.  $T_{1\rho, \text{adiab}}$  maps retain comparable map quality across repetitions with a nearly identical visual appearance of the maps. RefSL maps depict significant artifacts degrading the map quality in the myocardium, particularly in the second repetition.



**C. Overall performance:  $B_0$ -aSL vs. RefSL**

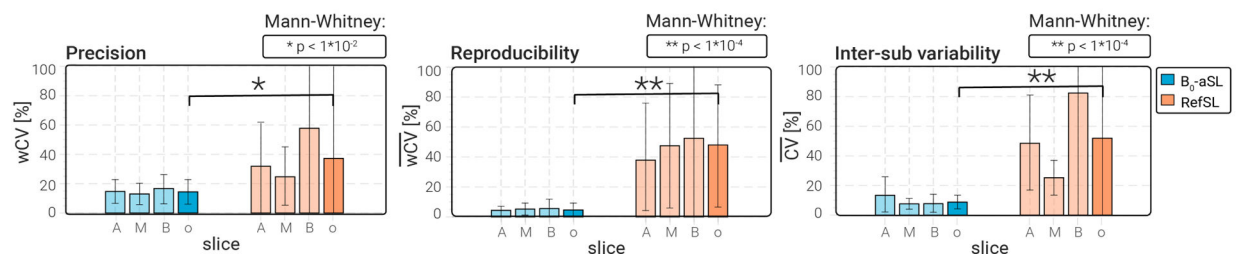


**Figure 8.**

(A) Bullseye plots showing the  $T_{1\rho, \text{adiab}}$  and  $T_{1\rho}$  values, averaged over all cohort 2 subjects and repetitions, for 16 AHA myocardial segments.  $T_{1\rho, \text{adiab}}$  values are consistently higher, but more homogeneous across the 16 segments for all preparations, compared with RefSL-based  $T_{1\rho}$  values. (B) Bullseye plots report the average precision ( $wCV$ ), reproducibility ( $w\bar{CV}$ ), and inter-subject variability ( $\bar{CV}$ ) coefficients for  $B_0$ -aSL-based  $T_{1\rho, \text{adiab}}$  maps and RefSL  $T_{1\rho}$  maps in 16 AHA myocardial segments. Global average values are reported at the center of each bullseye plot. Improved precision, reproducibility, and inter-subject variability are obtained with aSL preparations, compared to RefSL. (C) Bar plots comparing precision, reproducibility, and inter-subject variability for each preparation per slice and averaged across all slices (A=apical, M=mid-ventricular, B=basal, o=overall). Pair-wise statistical significance is marked by \* or \*\* and the corresponding p-values are shown on top of each plot. Significantly higher  $wCV_{r,i}$ ,  $w\bar{CV}$ , and  $\bar{CV}$  values are measured for conventional RefSL-based  $T_{1\rho}$  mapping compared with  $T_{1\rho, \text{adiab}}$ .

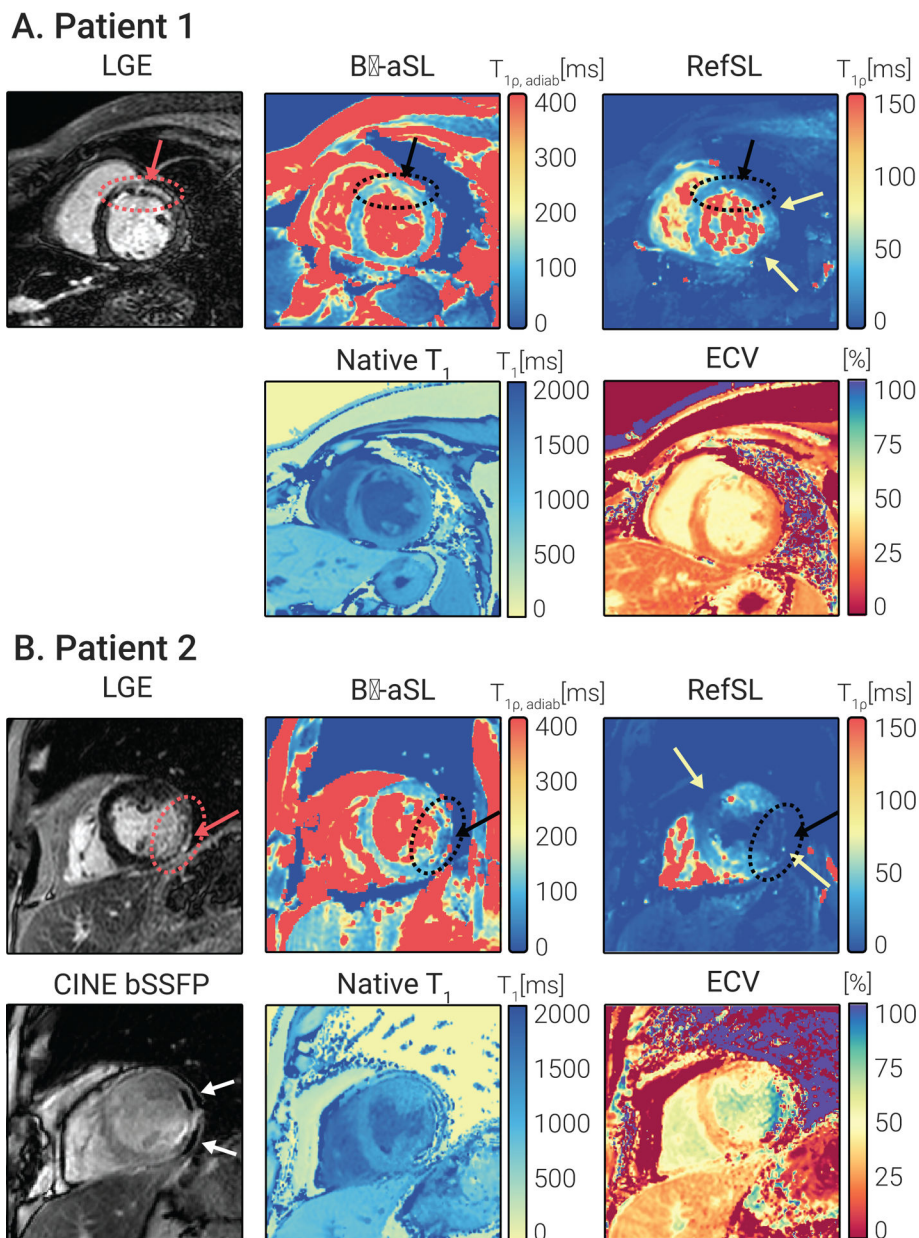


**Figure 9.**

(A) 53-year-old female patient suffering from ischemic cardiomyopathy. LGE images demonstrate near transmural (51–75%) enhancement of the mid anteroseptal and anterior wall and all apical wall segments with subendocardial extension into the basal anterior and anteroseptal segments and mid inferoseptum (black arrow). The  $B_1$ -aSL-based  $T_{1\rho, \text{adiab}}$  map shows elevation co-localized with LGE positive regions ( $T_{1\rho, \text{adiab}} = 146.24 \pm 25.34$ scar,  $99.40 \pm 11.58$  remote). Native  $T_1$  and  $T_2$  times are also focally elevated in the anteroseptal segment. Due to mapping inhomogeneity in the anterior and lateral regions (red arrows), no focal alteration is unambiguously identified in the conventional  $T_{1\rho}$  maps. (B) 59-year-old male patient with a history of ischemic cardiomyopathy. LGE images demonstrate transmural myocardial enhancement in the basal to mid-anterolateral segments, basal to mid-

inferolateral segments, and apical lateral segments (black arrow). Chemical shift artifacts in the bSSFP CINE images indicate lipomatous metaplasia.  $T_{1\rho, \text{adiab}}$  values decrease in the scar region ( $T_{1\rho, \text{adiab}} = 67.06 \pm 14.69$  scar,  $96.57 \pm 15.03$  remote). In this patient, significant artifacts obfuscate any potential focal alteration in the RefSL-based  $T_{1\rho}$  maps (red arrows).

Author Manuscript

Author Manuscript

Author Manuscript

Author Manuscript

**TABLE 1**

Adiabatic spin-lock preparations design parameters

Module name	Pulse shape			Design region			Performance	
	$\beta$	$f_{\max}$ [HZ]	$\tau_{\text{HS}}$ [ms]	$B_1^{\max}$ [ $\mu T$ ]	$\omega_1^{\text{off}}$ [Hz]	$\zeta_1$	SAR [W/kg]	Efficiency <sup>†</sup>
8HS-aSL	2.1	550	7.5	13.5	-150, ... +150	0.5, ... 1.0	<1.2	0.88
4HS-aSL	3.7	300	15	13.5	-150, ... +150	0.5, ... 1.0	<1.1	0.92
$B_0$ -aSL (2HS-aSL)	6.9	450	30	13.5	-200, ... +200	0.75, ... 1.0	<1.0	0.99
Bal-aSL (2HS-aSL)	5.5	350	30	13.5	-150, ... +150	0.5, ... 1.0	<1.0	0.98
$B_1$ -aSL (2HS-aSL)	4.4	200	30	13.5	-100, ... +100	0.25, ... 1.0	<1.1	0.94

<sup>†</sup> $M_x(\tau_{\text{SL}})/M(0)$  averaged over design region.

Author Manuscript

Author Manuscript

Author Manuscript

Author Manuscript